# Spin-Orbit and Core-Shielding Effects on Double-Excitation Resonances of Zn

L.-R. Wang,[1,2] H.-C. Chi,[3] and K.-N. Huang[1,2]
[1]*Institute of Atomic and Molecular Sciences, Academia Sinica, P.O. Box 23-166, Taipei, Taiwan 106, Republic of China*
[2]*Department of Physics, National Taiwan University, Taipei, Taiwan 106, Republic of China*
[3]*Department of Mathematics and Science Education, National Hualien Teachers College, 123 Huaci Road, Hualien, Taiwan 970, Republic of China*
(Received 8 March 1999)

Autoionization resonances of doubly excited states in the photoionization spectrum of the neutral Zn atom are calculated by using the multiconfiguration relativistic random-phase approximation theory. The cross section, angular distribution, and spin polarization of photoelectrons from the valence subshell $4s$ show strong dependence both on the spin-orbit and the core-shielding effects, and good agreements are obtained with available experimental measurements.

PACS numbers: 32.80.Fb, 32.70.Jz, 32.80.Dz

Low-energy photoionization spectrum of the neutral zinc atom has attracted much attention in recent years because the interplay between relativistic and correlation effects plays an important role. The absorption spectrum of the neutral zinc atom between photon energies 10.781 and 17.712 eV was first investigated by Beutler and Guggenheimer [1] in 1933. Absolute photoionization cross sections were reported by Marr and Austin [2], in which autoionization resonances arising from the singly excited states were measured. Theoretical works for this process have been performed using the nonrelativistic random-phase approximation by Amusia *et al.* [3] and the relativistic random-phase approximation by Johnson *et al.* [4]. In the lower energy region, the autoionization resonances arising from the singly excited states of the $3d$ electrons were calculated by Fliflet and Kelly [5] using many-body perturbation theory. The cross section near the $4s$ threshold was calculated by Shorer and Dalgarno [6] using the relativistic random-phase approximation.

However, it was not until 1978 that the autoionization resonances arising from doubly excited states of valence electrons of zinc were observed by Mansfield and Connerade [7], in which at least 35 doubly excited states were measured in the photoabsorption spectrum between 12.524 and 15.213 eV photon energies. Among these doubly excited states, a few were calculated by Bartschat [8] using a semirelativistic $R$-matrix method. More recently, five Rydberg series $4p_{1/2}ns_{1/2}$, $4p_{1/2}nd_{3/2}$, $4p_{3/2}ns_{1/2}$, $4p_{3/2}nd_{3/2}$, and $4p_{3/2}nd_{5/2}$ of autoionization resonances corresponding to doubly excited states were studied by Hwang *et al.* [9] using the multiconfiguration relativistic random-phase approximation theory (MCRRPA) [10,11]. Positions and profiles of these autoionization resonances in the photoionization spectrum were in general agreement with the experimental results.

In the present work, we investigate the photoionization spectrum of zinc in the region of interest by using the MCRRPA including core-excitation channels from the $3d$ and $3p$ subshells and thus provide an *ab initio* treatment of the core-shielding (CS) effects due to $3d$ and $3p$ electrons, which were omitted in our previous results. In contrast to the relativistic random-phase approximation theory (RRPA) [12], the MCRRPA takes into account not only the usual RPA-type correlations but also the important two-particle two-hole correlations with the doubly excited states by using a multiconfiguration wave function as its reference state.

Relatively strong spin-orbit couplings between electrons in the neutral zinc atom make its photoionization spectrum considerably more complex than that of Be or Mg. Two Rydberg series $4p_{1/2}ns_{1/2}$ and $4p_{1/2}nd_{3/2}$ which converge to the $4p_{1/2}$ threshold are disturbed by the close-by Rydberg series $4p_{3/2}ns_{1/2}$, $4p_{3/2}nd_{3/2}$, and $4p_{3/2}nd_{5/2}$ converging to the fine-structure companion $4p_{3/2}$ threshold. In fact, doubly excited states $4p_{3/2}ns_{1/2}$ ($n \leq 14$), $4p_{3/2}nd_{3/2}$ ($n \leq 10$), and $4p_{3/2}nd_{5/2}$ ($n \leq 10$) are below the $4p_{1/2}$ threshold and mix strongly with the doubly excited states $4p_{1/2}ns_{1/2}$ and $4p_{1/2}nd_{3/2}$ through spin-orbit as well as Coulomb interactions. The positions and widths of these autoionization resonances are influenced greatly by couplings between Rydberg series converging to these two fine-structure thresholds.

With increasing availability of synchrotron radiation as a light source, photoelectron angular distributions as well as cross sections from individual subshells of atoms or ions are determined. Measurement on the photoelectron angular distribution of zinc made by Brehm and Pfeiffenberger-Pertl [13] has shown that the angular distribution parameter $\beta$ varies from 2 to $-1$ in the vicinity of autoionization resonances arising from the excitation of $3d$ electrons. This experiment was a striking demonstration of the importance of relativistic effects on the photoionization process of the neutral zinc atom. Cross sections depend on the size of the transition amplitudes of contributing channels, while the angular distributions are sensitive to relative phases between channels. In the vicinity of doubly excited states, our calculations indicate that the cross sections and $\beta$ parameters are extremely sensitive both to the spin-orbit and CS effects. Furthermore, for a complete understanding of low-energy

 0031-9007/99/83(4)/702(4)$15.00 

photoionization, the determination of spin polarization of photoelectrons is required in addition to cross sections and angular distributions [14–16]. Therefore, spin polarization parameters of photoelectrons are also calculated in the present calculation.

The MCRRPA theory and its applications have been reviewed in a previous paper [17], and only a summary of the essential features will be given here. The MCRRPA equations may be derived by linearizing the time-dependent multiconfiguration Dirac-Fock equations describing the response of an atom to a time-dependent external field. The ground reference state of the zinc atom in our calculation is represented by a multiconfiguration wave function as

$$\Psi = C_1(4s_{1/2}^2) + C_2(4p_{1/2}^2) + C_3(4p_{3/2}^2), \qquad (1)$$

where $(4l_j^2)$ denotes symbolically an antisymmetrized wave function constructed from two electrons in the valence orbital $4l_j$ and 28 electrons in seven core orbitals $1s_{1/2}$, $2s_{1/2}$, $2p_{1/2}$, $2p_{3/2}$, $3s_{1/2}$, $3p_{1/2}$, $3p_{3/2}$, $3d_{3/2}$, and $3d_{5/2}$. The coefficients $C_1$, $C_2$, and $C_3$ in Eq. (1) are configuration weights. Consequently, the valence-polarization effects due to the presence of $4p^2$ configurations are accounted for. The unperturbed orbitals and configuration weights are determined by solving the multiconfiguration Dirac-Fock equations [18]. The MCRRPA equations take into account all one-particle one-hole excitations of the ground reference state, and thereby two-particle two-hole final-state correlations are included in an *ab initio* manner.

In the present calculation, eighteen excitation channels in the electric-dipole approximation are considered. The excitation channels from the valence subshell $4s_{1/2}$ are *open* in the photon energies considered and produce the photoelectrons. The photoelectron coming out of the valence subshell $4s_{1/2}$ resonates with singly and doubly excited states represented, respectively, by the *closed* core- and valence-excitation channels. These excitation channels in the energy region of interest are summarized as follows.

(i) Open valence-excitation channels:

$4s_{1/2} \rightarrow \varepsilon p_{1/2}$ (channel 1), $4s_{1/2} \rightarrow \varepsilon p_{3/2}$ (channel 2).

(ii) Closed core-excitation channels:

$3d_{3/2} \rightarrow \varepsilon p_{1/2}$ (channel 3), $3d_{3/2} \rightarrow \varepsilon p_{3/2}$ (channel 4),
$3d_{3/2} \rightarrow \varepsilon f_{5/2}$ (channel 5), $3d_{5/2} \rightarrow \varepsilon p_{3/2}$ (channel 6),
$3d_{5/2} \rightarrow \varepsilon f_{5/2}$ (channel 7), $3d_{5/2} \rightarrow \varepsilon f_{7/2}$ (channel 8),
$3p_{1/2} \rightarrow \varepsilon s_{1/2}$ (channel 9), $3p_{1/2} \rightarrow \varepsilon d_{3/2}$ (channel 10),
$3p_{3/2} \rightarrow \varepsilon s_{1/2}$ (channel 11), $3p_{3/2} \rightarrow \varepsilon d_{3/2}$ (channel 12),
$3p_{3/2} \rightarrow \varepsilon d_{5/2}$ (channel 13),

These core-excitation channels account for the major CS effects due to $3d$ and $3p$ electrons.

(iii) Closed valence-excitation channels:

$4p_{1/2} \rightarrow \varepsilon s_{1/2}$ (channel 14), $4p_{1/2} \rightarrow \varepsilon d_{3/2}$ (channel 15),
$4p_{3/2} \rightarrow \varepsilon s_{1/2}$ (channel 16), $4p_{3/2} \rightarrow \varepsilon d_{3/2}$ (channel 17),
$4p_{3/2} \rightarrow \varepsilon d_{5/2}$ (channel 18).

These valence-excitation channels account for the major final-state correlations arising from Coulomb as well as spin-orbit interactions among valence electrons.

These closed core- and valence-excitation channels manifest themselves, respectively, as single- and double-excitation resonances in the photoionization spectrum of the $4s_{1/2}$ subshell of zinc.

Doubly excited states $4pns$ of zinc can be expanded by two major configurations $[4p_{1/2}ns_{1/2}]_1$ and $[4p_{3/2}ns_{1/2}]_1$ in *jj*-coupling scheme or $(4pns)\ ^3\mathrm{P}_1$ and $(4pns)\ ^1\mathrm{P}_1$ in *LS*-coupling scheme. Except for $4p5s$, doubly excited states $4snp$ ($n \geq 6$) are described more suitably in *jj* coupling than in *LS* coupling. We therefore adopt the *jj*-coupling notations in our results. Four separate calculations, denoted as (a), (b), (c), and (d), are performed by including increasingly more valence-excitation channels to analysis spin-orbit effects on resonance energies and widths of doubly excited states. In addition, all calculations are performed with and without core-excitation channels to demonstrate CS effects.

The energies $E_r$ and widths $\Gamma_r$ of double-excitation resonances obtained from the sum of eigenphase shifts with CS effects are listed in Table I. The widths of $4pns$ resonances are approximately 10 times larger than the $4pnd$ resonances because the doubly excited states $4pns$ and the continuum states $4s\varepsilon p$ have the same $sp$-orbital symmetry and therefore mix strongly. The width of the $4p_{3/2}4d_{3/2}$ resonance is comparable to that of the $4p_{1/2}6s_{1/2}$ resonance because of the strong mixing between these two doubly excited states. It is worth noting that the widths of all resonances decrease as the number of valence-excitation channels included in the calculation increases.

The resonance energies $E_r$ are in good agreement with the experimental results [7]. However, it should be noted that the resonance energies determined in the experiment for the $4p_{1/2}7s_{1/2}$, $4p_{1/2}5d_{3/2}$, $4p_{3/2}7s_{1/2}$, $4p_{3/2}5d_{3/2}$ resonances are measured at peaks of resonances, while for the $4p_{1/2}6s_{1/2}$, $4p_{3/2}7s_{1/2}$, and $4p_{3/2}4d_{3/2}$ resonances the experimental values are given at the greatest change of the cross section. In our calculation, we find that the positions of the window, the peak, and the greatest change of the cross section for a double-excitation resonance are quite close (about 0.006 eV apart, in average) to the position of the same resonance obtained from eigenphase shifts. Nevertheless, the experimental results shown in Table I have been modified to correct for this small variation in the positions of double-excitation resonances. The interference between two doubly excited states "repels" corresponding resonances apart, as shown in Fig. 1. In column (b), the $4p_{1/2}4d_{3/2}$ resonance "pushes" the $4p_{1/2}6s_{1/2}$ resonance to a higher energy, the new added $4p_{3/2}6s_{1/2}$

TABLE I. Resonance energies and widths for the autoionization states of Zn. Numbers in brackets indicate powers of 10. The MCRRPA calculations are performed including the CS effects of the $3d$ and $3p$ subshells.

| | Resonance energies $E_r$ (eV) | | | | | | Resonance widths $\Gamma_r$ (eV) | | | |
|---|---|---|---|---|---|---|---|---|---|---|
| | $R$-matrix [8] | MCRRPA | | | | Expt. [7] | MCRRPA | | | |
| | | (a) | (b) | (c) | (d) | | (a) | (b) | (c) | (d) |
| $4p_{1/2}6s_{1/2}$ | 14.150 | 14.1209 | 14.1455 | 14.1243 | 14.1078 | 14.122 | 6.356(−2) | 5.159(−2) | 3.736(−2) | 2.524(−2) |
| $4p_{1/2}7s_{1/2}$ | 14.680 | 14.6580 | 14.6677 | 14.6569 | 14.6478 | 14.674 | 2.655(−2) | 2.336(−2) | 2.152(−2) | 1.263(−2) |
| $4p_{1/2}4d_{3/2}$ | 13.225 | | 13.9414 | 13.9433 | 13.8622 | | | 3.816(−3) | 2.386(−3) | 6.732(−4) |
| $4p_{1/2}5d_{3/2}$ | 14.340 | | 14.5751 | 14.5767 | 14.5568 | 14.522 | | 1.511(−3) | 1.298(−3) | 8.523(−4) |
| $4p_{3/2}6s_{1/2}$ | | | | 14.2295 | 14.2364 | 14.268 | | | 1.167(−1) | 9.752(−2) |
| $4p_{3/2}7s_{1/2}$ | | | | 14.7667 | 14.7673 | 14.759 | | | 4.334(−2) | 3.672(−2) |
| $4p_{3/2}4d_{3/2}$ | | | | | 14.0380 | 14.028 | | | | 7.027(−3) |
| $4p_{3/2}5d_{3/2}$ | | | | | 14.6752 | 14.683 | | | | 6.523(−3) |
| $4p_{3/2}4d_{5/2}$ | | | | | 14.1536 | | | | | 1.268(−2) |
| $4p_{3/2}5d_{5/2}$ | | | | | 14.7173 | | | | | 3.530(−3) |

(a) MCRRPA calculation including closed valence-excitation channel (14).
(b) MCRRPA calculation including closed valence-excitation channels (14) and (15).
(c) MCRRPA calculation including closed valence-excitation channels (14), (15), and (16).
(d) MCRRPA calculation including closed valence-excitation channels (14), (15), (16), (17), and (18).

resonance "lowers" the $4p_{1/2}6s_{1/2}$ resonance in energy, and the $4p_{3/2}4d_{3/2}$ resonance lowers the $4p_{1/2}4d_{3/2}$ resonance dramatically. We note that the differences between results with and without core-excitation channels are less than 0.001 eV in most cases, and this indicates that CS effects on the resonance energies and widths are almost negligible.

The CS effects, however, change the shape of cross-section curves considerably, as shown in Fig. 2. The asymmetry $q$ parameters of the resonance profile [19] for the $4p_{1/2}6s_{1/2}$ resonance in plate (a) are 0.96 and 2.57, respectively, without and with CS effects. For a given width of the resonance, the $q$ parameter measures the ratio between the transition probabilities to the bound and to the continuum components of the final state from the initial state. If the resonance is dominated by the contribution from the transition to the bound component of the final state, its $q$ value is large, and this reduces the cross section at shoulders of the resonance. The cross section far from a resonance is mainly due to the transition probability from the initial state to the continuum part of the final state. Closed core-excitation channels cause the $3d^9 4s^2 4p\ ^3\mathrm{D}_1$ and $3d^9 4s^2 4p\ ^3\mathrm{P}_1$ resonances in the photon energies between 11.587 and 12.155 eV [2]. These single-excitation resonances have very large $q$ values and therefore generally reduce the background contribution to the double-excitation resonances

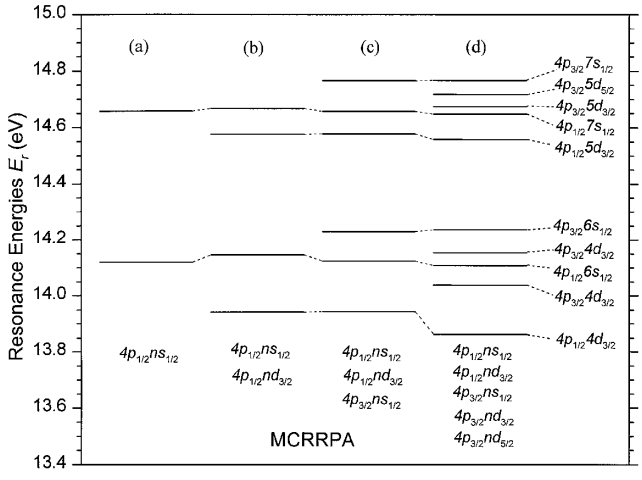


FIG. 1. Double-excitation resonance energies $E_r$ in the photoionization spectrum of the neutral zinc atom. Results from four separate MCRRPA calculations, (a), (b), (c), and (d), with increasingly more valence-excitation channels as indicated in Table I are presented.

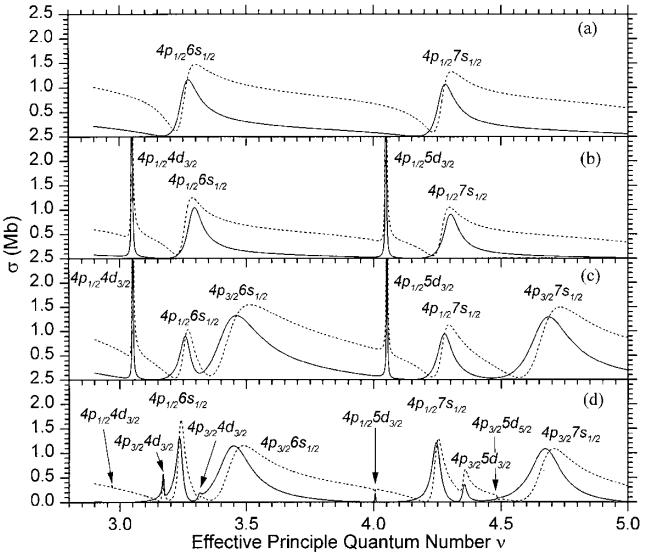


FIG. 2. Photoionization cross section $\sigma$ of the neutral zinc atom as a function of the effective principle quantum number $\nu$. Result from four separate MCRRPA calculations (a), (b), (c), and (d) are presented. Dashed curves are for the MCRRPA calculations without CS effects, and solid curves are for the MCRRPA calculations with the CS effects of the $3d$ and $3p$ subshells.

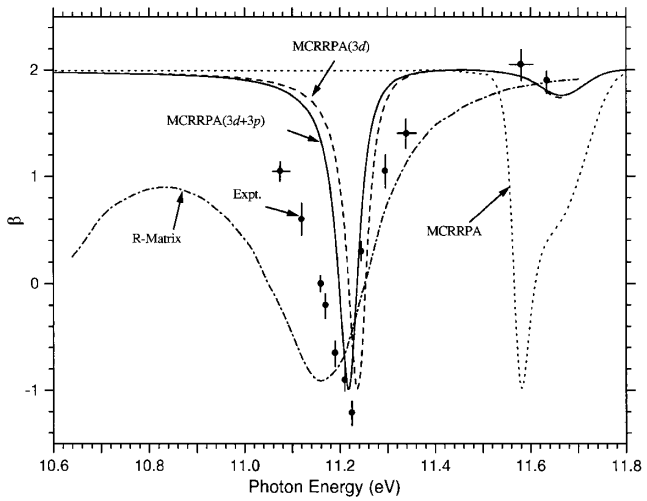


FIG. 3. Asymmetry parameter $\beta$ as a function of the photon energy: $\cdots$ MCRRPA calculation without CS effects; – – – MCRRPA($3d$) calculation with the CS effects of the $3d$ subshells; — MCRRPA($3d + 3p$) calculation with the CS effects of the $3d$ and $3p$ subshells; –· –· $R$-matrix calculation [8]; ♦ Experimental data [13].

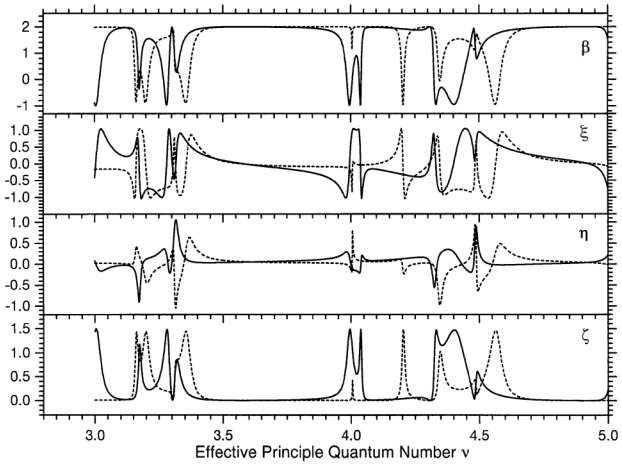


FIG. 4. Asymmetry parameter $\beta$, spin-polarization parameters $\xi$, $\eta$, and $\varsigma$ as a function of the effective principle quantum number $\nu$: $\cdots$ MCRRPA calculation without CS effects; — MCRRPA calculation with the CS effects of the $3d$ and $3p$ subshells.

nearby. This, in turn, causes the raising of the $q$ parameter for the double-excitation resonances and makes these resonances more symmetric, as shown in Fig. 2. In an extreme case, the $4p_{1/2}5d_{3/2}$ resonance is nearly a window resonance ($q \sim 0.08$) without CS effects but a peak resonance ($q \sim 16$) with CS effects. We note that the main CS effects in this region are due to the excitation of $3d$ electrons and the correlations from the excitation of $3p$ electrons are very small.

Our results for the asymmetry parameter $\beta$ for the angular distribution of photoelectrons in the region above the $4s_{1/2}$ threshold are plotted in Fig. 3 as a function of the photon energy. We find that the $\beta$ parameter from the MCRRPA including the CS effects arising from the excitation of the $3d$ and $3p$ electrons reaches its minimum value of $-1$ at $\hbar\omega = 11.22$ eV, in excellent agreement with the experimental result [13] 11.22 eV. Results of the $R$-matrix method [8] for $\beta$ are also plotted in Fig. 3. The minimum position of $\beta$ in the $R$-matrix calculation is at $\hbar\omega = 11.16$ eV which is close to our result as well as the experimental measurement, but its trend in the lower photon-energy region seems to depart from either. The $\beta$ curves from the MCRRPA without and with partial CS effects are presented to demonstrate the importance of CS effects on the asymmetry parameter $\beta$. The position of the dip in the $\beta$ curve is improved by including the excitation channels from the $3p$ subshells. However, the dips in our $\beta$ curves are much narrower than those of the experiment [13], and this is probably due to additional core-polarization effects of the ground reference state omitted in our calculation. The asymmetry parameter $\beta$ and spin-polarization parameters $\xi$, $\eta$, and $\varsigma$ in the double-excitation resonance region are plotted in Fig. 4. The expressions of $\beta$, $\xi$, $\eta$, and $\varsigma$ in terms of multipole-transition amplitudes have been given previously [14]. They all show a strong dependence on CS effects, which are primarily due to the excitation of the $3d$ electrons. These parameters, sensitive to the interplay between correlation and relativistic effects, can provide both a critical comparison and a stringent test of theories.

[1] J. Beutler and K. Guggenheimer, Z. Phys. **87**, 176 (1933).
[2] G. V. Marr and J. M. Austin, J. Phys. B **2**, 107 (1969).
[3] M. Y. Amusia, V. K. Ivanov, N. A. Cherepkov, and L. V. Chernysheva, Sov. Phys. JETP **39**, 752 (1975).
[4] W. R. Johnson, V. Radojevic, Pranawa Deshmukh, and K. T. Cheng, Phys. Rev A **25**, 337 (1982).
[5] A. W. Fliflet and H. P. Kelly, Phys. Rev. A **13**, 312 (1976).
[6] P. Shorer and A. Dalgarno, Phys. Scr. **21**, 432 (1980).
[7] M. W. D. Mansfield and J. P. Connerade, Proc. R. Soc. London A **359**, 389 (1978).
[8] K. Bartschat, J. Phys. B **20**, 5023 (1987).
[9] C.-Y. Hwang, H.-C. Chi, and K.-N. Huang, Phys. A **44**, 7189 (1991).
[10] K.-N. Huang and W. R. Johnson, Phys. Rev. A **25**, 634 (1982).
[11] W. R. Johnson and K.-N. Huang, Phys. Rev. Lett. **48**, 315 (1982).
[12] W. R. Johnson and K. T. Cheng, Phys. Rev. A **20**, 978 (1979).
[13] B. Brehm and H. Pfeiffenberger-Pertl, Z. Phys. A **320**, 37 (1985).
[14] K.-N. Huang, Phys. Rev. A **22**, 223 (1980); **26**, 3637 (1982).
[15] U. Heinzmann, G. Schönhense, and J. Kessler, Phys. Rev. Lett. **42**, 1603 (1979).
[16] K.-N. Huang, W. R. Johnson, and K. T. Cheng, Phys. Rev. Lett. **43**, 1658 (1979).
[17] K.-N. Huang, H.-C. Chi, and H.-S. Chou, Chin. J. Phys. **33**, 565 (1995).
[18] J. P. Desclaux, Comput. Phys. Commun. **9**, 31 (1975).
[19] U. Fano, Phys. Rev. A **124**, 1866 (1961).